Numerical simulation of mixed convection heat transfer of fluid in a cavity driven by an oscillating lid using lattice Boltzmann method

H. Lamarti, M. Mahdaoui, R. Bennacer, A. Chahboun

Version of Record: https://www.sciencedirect.com/science/article/pii/S0017931018356825
Manuscript_c2f1c45a4f8a24d382846df9ab85a96b

Numerical simulation of mixed convection heat transfer of fluid in a cavity driven by an oscillating lid using lattice Boltzmann method

H. Lamarti[1], M. Mahdaoui[1], R. Bennacer[3], and A. Chahboun[1]

[1]FST, University of Abdelmalek Essaadi, Tangier, Morocco
[3]LMT/ENS - Cachan/CNRS/University Paris Saclay, 94235 Cachan,France

March 9, 2019

Abstract

Lattice Boltzmann Method (LBM) has been applied for the simulation of a mixed convection heat transfer of two dimensional Newtonian fluid in a square cavity driven by a periodically oscillating lid. The top wall is maintained at higher variable temperature. The developed LBM code in Matlab, is applied for the oscillating lid to simulate the fluid flow and heat transfer in cavity, was validated using various Reynolds and Grashof numbers. Nusselt number was calculated for various pertinent dimensionless groups. Fluid flow and heat transfer characteristics were examined in the domain of Reynolds number, Grashof number, the dimensionless lid oscillation frequency and different values of temperature. Such that: $10^2 \leq Re \leq 10^3$, $10^2 \leq Gr \leq 10^6$, $0.1 \leq \omega \leq 5$, *the Prandtl number was fixed as* 0.71. *The results show that the variation of the Reynolds and Grashof numbers has an effect on energy transport process and drag force behavior depending on the conduct of the velocity cycle. Moreover the variation of Rayleigh number and period of the heated portion has an effect on the transfer rate on convective structures.*

I. Introduction

Mixed convection heat transfer in a cavity due to the interaction of the buoyancy force with shear forces has received a lot of attention from the researchers. This problem is often encountered in industrial processes such as glass production, food processing and nuclear reactors. A such phenomenon is also observed in our body through the motion of joints. In nature, it's observed, as convective thermal cur- rents that occur in lakes and rivers. This type of problem has been addressed in the literature. In fact, Iwatsu et al.[1] have performed a numerical study of a two-dimensional flow in a cavity driven by a unidirectional movement and a vertical temperature gradient. They produced models similar to mixed convection flows when incorporating small numerical numbers of Richardson. It is widely used as a reference for the evaluation of different numerical schemes. Prasad et al.[2] reported experimental results on the mixed-convection heat transfer process in a lid cavity for a Richardson number range between 0.1 and 1000. They concluded that the heat transfer mechanism is a weak Richardson's number function in relation to the number of Reynolds considered and to the values of the physical aspect ratio. However, the effect of an oscillating lid on mixed convection heat transfer has received less attention from researchers. Khanafer et al. [3] have made a numerical study of unsteady laminar convective heat transfer in a cavity driven by

a sinusoidal lid using a finite element scheme based on the Galerkin method of weighted residuals. The obtained results reveal that the Reynolds number and Grashof number would either enhance or retard the energy transport process and drag forces behavior depending on the conduct of the velocity cycle. Recently, lattice Boltzmann method (LBM) emerged as an alternative powerful method for solving fluid dynamics problems. The fundamental idea of LBM is to describe a fluid as an ensemble of many particles interacting locally at the nodes of a regular lattice by collisions and then the particles move only along the lattice and collide again with other particles once they arrive to the nodes [4] It can be programmed naturally for parallel processing machines. It's important to situate its performance compared to conventional numerical methods to simulate and reproduce the isothermal or thermal fluid flows. Among the published papers in the field of mixed convection heat transfer using LBM, we can cite Bennacer et al.[4] who have applied a moment LB model different from the Lattice of Bhatnagar, Gross and Krook $(LBGK)$ approximation to investigate a situation combining natural and forced convection for lid driven in a two-dimensional square cavity over a much wider range of Rayleigh and Reynolds numbers. Houat et al.[5] have presented a numerical study of the laminar mixed convection in a square cavity with two opening. They proposed the LBM with a double population model for resolving the thermal fluid flow in cavity. The obtained results are compared with the conventional method, especially Finite Volume Method results. These results confirm that the thermal lattice Boltzmann method $(TLBM)$ model has the advantage of good numerical stability and the ability to manage the overall heat transfer by convection problems. In view of previous studies, it is clear that no research has been conducted in the field of mixed convection heat transfer in cavities driven by periodic wall movement using LBM. Recently, the potential to use oscillatory flows to increase the rate of heat transfer for example: Stirling machines, Cryocoolers and electronic components has renewed interest in the field. Progress in under-standing heat transfer in oscillatory flows (alternative flow) is incomplete [6]. In the present study, we applied $TLBM$ to simulate a mixed convection heat transfer of flow two-dimensional inside in a cavity driven by a periodic oscillation using the Matlab program. We first validated the Moment Lattice Boltzmann Model $(MLBM)$ simulation for different Reynolds and Grashof numbers compared to reference [1],[3] solutions in the literature, then we studied the phenomena observed for different Reynolds and Grashof numbers and oscillation frequencies.

II. Methods

i. Problem description

A square cavity is assumed, the upper wall is maintained at a high temperature T_{hot} and the lower wall and the two lateral walls are adiabatic T_{cold} . The side and bottom walls of the cavity are stationary as shown in Figure (1) . The velocity of the upper wall in the x direction is given by [7]:

$$U_{lid} = U_{max} cos(\omega t) \tag{1}$$

U_{max} : maximum speed of the upper wall. t : time. ω : frequency of oscillation. It is assumed that the fluid is Newtonian and the flow is laminar. In addition, it is assumed that the isothermal, incompressible and $2D$ flow with constant fluid properties. In this study, The Rayleigh number defined as: $Ra = g\beta\Delta TN^3/\kappa\nu$,where N is the space node number, g is acceleration due to gravity and β is the thermal expansion coefficient ,The Grashof number defined as: $Gr = Ra/Pr$ takes values between 10^2 and 10^6 , the Prandtl number is fixed by: $Pr = \nu/\kappa$, is equal to 0.71. The Reynolds number defined as: $Re = U_{max}H/\nu$, where: ν is the kinematic viscosity of fluid and κ is thermal diffusion. To find a suitable grid that leads to the autonomous results from grid and in order to determine the appropriate grid size, the average Nusselt number with various grid point numbers of $Re = 100$ is presented in Table (1).

Number of points	Nu
60×60	1.9348
80×80	1.9423
100×100	1.9469
120×120	1.9508

Table 1: *The average Nusselt number on the hot wall at Re=100 and Gr=100*

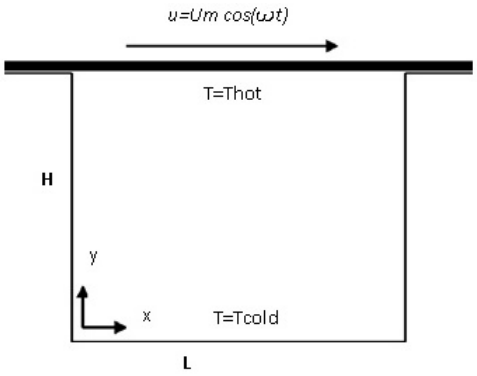

Figure 1: *Schematic representation of cavity flow driven by an oscillating lid*

As can be seen, the discrepancy of the average Nusselt number between the grid with 80×80 points and the grid with 100×100 points is about 0.2%. So the grid with the 100×100 points is selected as the optimal grid. The Re values considered For the simulations is: 100, 400 and 1000. The oscillation frequencies are: 0.1, 1 and 5 (dimensionless lid frequency) [3].

ii. LBM NUMERICAL METHOD

LBM is based on a microscopic model but is used to simulate macroscopic fluid properties such as density, velocity and temperature. The fundamental idea of *LBM* is to describe a fluid as an ensemble of many particles interacting locally at the nodes of a regular lattice by collisions, and then the particles move only along the lattice and collide again with other particles once they arrive at the nodes. During the movement, the momentum and the energy are transported. This discrete microscopic model can be proved to recover the conservation laws of continuum fluid dynamics, and, thus, allows the computation of the macroscopic variables such as density and velocity. The researches mentioned above were carried out with either macroscopic method or mesoscopic method which usually refers to *LBM*. In recent years this approach has drawn more and more attention, since it's easy to study complex boundary condition and it is suitable for parallel calculation. It could be used to investigate phase separation (e.g. Vladimirova et al.(1999) [8], Suppa et al. (2002)[9], Xu et al. (2003) [10]), diffusion (Shan et al. (1995) [11]), wetting (Raiskinmaki et al. (2000) [12], Iwahara et al. (2003) [13]), evaporation (Palmer et al. (2000) [14]), particle-fluid suspensions (Ladd (1994) [15][16]), flow in porous media (Succi et al. (1989) [17], Heijs et al. (1995) [18]), heat transfer and phase change (Alexander and al. (1993) [19], He and al. (1998) [20], Tang and al. (2003) [21], Semma and al (2007) [22]). There are mainly three LBM models for heat transfer simulation: multi-speed model (McNamara et al. (1993) [23], Alexander et al. (1993) [19], Chen et al. (1994) [24]), double-distribution function model (He et al. (1998) [20]) and Hybrid-finite-difference model (Raoyang Zhang et al. (2003) [25], Mezrhab and al. (2004) [26]). In the Hybrid-Finite-difference model, the temperatures are obtained by solving discrete macro energy equation with finite-difference method, during which the velocity is calculated by *LBM*. In multi-speed model, the internal energy is involved in the density distribution function, and the temperature can be expressed with the distribution function just as velocity. This model has a poor stability. In contrary, in double-distribution function model, besides the density distribution function there is another distribution function "energy distribution function", based on which the internal energy equation evolution can be developed. The form of the energy distribution function is as same as that of the density distribution except that it is scalar quality while the latter is a vector.

The particles distribution Boltzmann equation

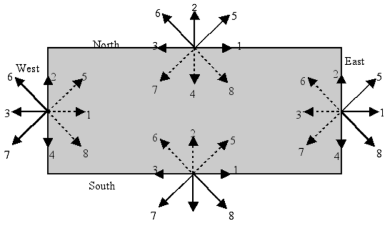

Figure 2: *The two-dimensional and nine velocity D2Q9 model*

is expressed in $D2Q9$ momentum model as:

$$\frac{\partial f}{\partial t} + c\nabla f = (\frac{\partial f}{\partial t})_{scat} \tag{2}$$

Where, $f(x, c, t)$ is the distribution function, which is the function of particle velocity c at location x and at time t. The right hand side in Equation (2) represents the diffusion process when the new equilibrium distribution is rebuilt after the collision. In general, this term is nonlinear and there are different methods to address it. Based on $D2Q9$ model (as shown in figure (2)), where the state of the fluid at the location x and at the time t is defined as $F(x,t) = f_1(x,t), f_2(x,t), .., f_8(x,t)$ with a vector of particles populations $f_i(i = 0, 1, ..., 8)$. The discrete distribution equation is as follows:

$$f_i(x + c_i\Delta t, t + \Delta t) - f_i(x,t) = (\Omega F)_i \tag{3}$$

Where, the micro discrete velocities c_i are respectively equal to 0 for $i = 0, 1$ for $(i = 1, 2, 3, 4)$, and $sqrt(2)$ for $(i = 5, 6, 7, 8)$, where i refers to the discrete velocity direction as represented in figure (2). F is the space vector based on the discrete velocity set. Ω is the collision operator, it can be represented in different formula based on different approximation and one of the method would be introduced later.

ii.1 LB moment model

one can interpret the dynamics of the model as a succession of two steps: propagation of particles from nodes to their neighbors and collision or redistribution between the various velocities c_i at each lattice node. In this article, The adapted $D2Q9$ model combines the vector space and the moment space. That is, as mentioned above, the state of the fluid at location x and time t is defined with a vector of 9 dimensions so that a $9N$ dimensional vector space$F = R^{9N}$ could be constructed based on the discrete velocity set c_i, where N is the space node number. At the same time, a space $M = R^{9N}$ could also be constructed based on the moments of f_i. Obviously, there are 9 independent moments for the discrete velocity set at each lattice node. One should notice that in real space F it is easy to handle the propagation step of the evolution in Equation (2), whereas Mezrhab et al.(2007) [26] pointed out that it is preferably to treat the collision part of the equation in M space. The relationship between the two spaces is (d'Humieres (1992) [27]):

$$m = Mf \tag{4}$$

Where the coefficients a_{ij} in the M matrix are constructed from the velocities c_i , and must not be singular as the following (Mezrhab et al. (2004) [28], Tekitek et al. (2006) [29]):

$$M = \left|\begin{array}{ccccccccc|c} 1 & 1 & 1 & 1 & 1 & 1 & 1 & 1 & 1 & \rho \\ 0 & 1 & 0 & 1 & 0 & 1 & 1 & 1 & 1 & j_x \\ 0 & 0 & 1 & 0 & 1 & 1 & 1 & 1 & 1 & j_y \\ -4 & -1 & -1 & -1 & -1 & 2 & 2 & 2 & 2 & E \\ 0 & 0 & -2 & 0 & 2 & 1 & 1 & -1 & -1 & \epsilon \\ 4 & -2 & -2 & -2 & -2 & 1 & 1 & 1 & 1 & T_{xx} \\ 0 & 1 & -1 & 1 & -1 & 0 & 0 & 0 & 0 & T_{yy} \\ 0 & 0 & 0 & 0 & 0 & 1 & -1 & 1 & -1 & \Phi_x \\ 0 & -2 & 0 & 2 & 0 & 1 & -1 & -1 & 1 & \Phi_y \end{array}\right| \tag{5}$$

Where, the signals on the right line beside the matrix are corresponding to the physical modes calculated from every row based on Equation (4). That is to say, the first row in the matrix allows to compute the density ρ ; the second and third rows are for the x and y components of momentum (mass flux) j_x and j_y . E is related to the kinetic energy, ϵ is related to the square of the energy. T_{xx} and T_{yy} correspond to the diagonal and off-diagonal components of the stress tensor. Φ_x and Φ_y are the x and y components of the energy flux. Now it comes to define the collision operator Ω. It is known that the collision step would not modify the moments such as mass, energy

and linear momentum if there is no body force. Therefore, these conserved moments satisfy:

$$m_0^{ac} = m_0^{bc} = \rho \tag{6}$$

$$m_1^{ac} = m_1^{bc} = j_x \tag{7}$$

$$m_2^{ac} = m_2^{bc} = j_y \tag{8}$$

Where m_j^{ac} and m_j^{bc} are respectively the moments after collision and before collision. For the non-conserved moments, the collision and relaxation process can be expressed as:

$$m_j^{ac} = m_j^{bc} + s_j(m_j^{eq} - m_j^{bc}) \tag{9}$$

Where s_j is a relaxation rate. For stability reasons, it is necessary to take the relaxation rates between 0 and 2, and m_j^{eq} is the value of the moment j when the system reaches equilibrium. Though the local energy conservation is destroyed by collision, the total energy is conserved. The values of moments when the system is at equilibrium are (Shankar et al. (2000) [30]):

$$m_3^{eq} = 6(C_s^2 - 4)\rho + \frac{j_x^2 + j_y^2}{\rho} \tag{10}$$

$$m_4^{eq} = \frac{j_x^2 - j_y^2}{\rho} \tag{11}$$

$$m_5^{eq} = \frac{j_{x\times y}}{\rho} \tag{12}$$

$$m_6^{eq} = -j_x \tag{13}$$

$$m_7^{eq} = -j_y \tag{14}$$

$$m_3^{eq} = \rho - \frac{j_x^2 + j_y^2}{\rho} \tag{15}$$

This model was applied to study a viscous fluid with speed of sound $c_s = 1/sqrt(3)$ and kinematics shear viscosity $\nu = 1/3(1/s_4 - 1/2)$. It is found that too large mean velocity of the model could induce numerical instabilities. In practical the velocity should not exceed 0.2 in the whole fluid domain. If this is satisfied, the velocity dependent corrections to the continuous Navier-Stokes equations are quite small. Numerous tests prove that this LB moment model provides a satisfactory second order simulation technique.

ii.2 LB for temperature field

The double distribution functions are adapted to simulate the temperature. A same moment model is applied except that the first moment described the last session to calculate density turns to calculate temperature, the collision. The relaxation step becomes related to node velocity obtained by last session. Therefore, the interaction of velocity and temperature is realized in a computational way. To save the calculation time, a $D2Q5$ model is used for energy equation instead of the $D2Q9$ model. The simulation results expressed later would show that this simplifying method is effective. Because of temperature difference between the two vertical walls, the buoyancy $f = aT(x,t)$ is produced in the direction of y direction. Where a is equal to $g\beta$ and it plays the role of $g\beta$ in a real fluid, g being the acceleration due to gravity and β being the thermal expansion coefficient. The buoyancy is acting as a body force and modifies the linear momentum conservation in the collisions. Thus the formulas (7) and (8) turn to:

$$m_1^{ac} = m_1^{bc} + f_x \tag{16}$$

$$m_2^{ac} = m_2^{bc} + f_y \tag{17}$$

where f_x and f_y are respectively the x and y components of the body force. Obviously, in view of simulation method, temperature and velocity are associated. We define the average Nusselt number as (R. Bennacer [4]):

$$Nu = \frac{1}{k2\Delta TN}\sum v_y r_{ij} T(r_{ij}) - 1 \tag{18}$$

Note that the value of ΔT may be taken as 1. The Strouhal number is often given as:

$$St = \frac{fH}{U_{max}} \tag{19}$$

where f is the frequency of vortex shedding, H is the characteristic length and Um is the flow velocity.

ii.3 Algorithm validation

Figure (3) shows the v_x and v_y velocities along the mid-sections in the x and y directions for

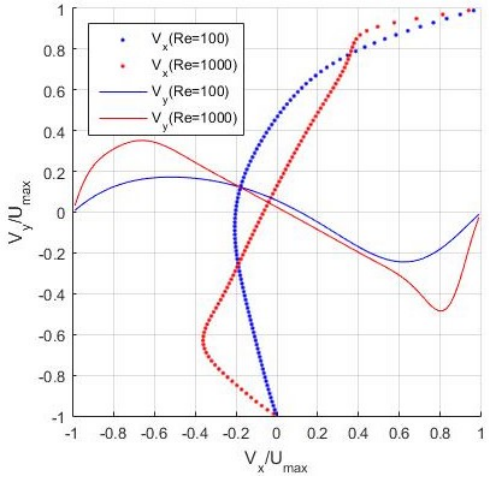

Figure 3: *v_x and v_y velocity components on the vertical and horizontal mid-planes for $Re = 10^2$ and 10^3 at $Gr = 10^2$*

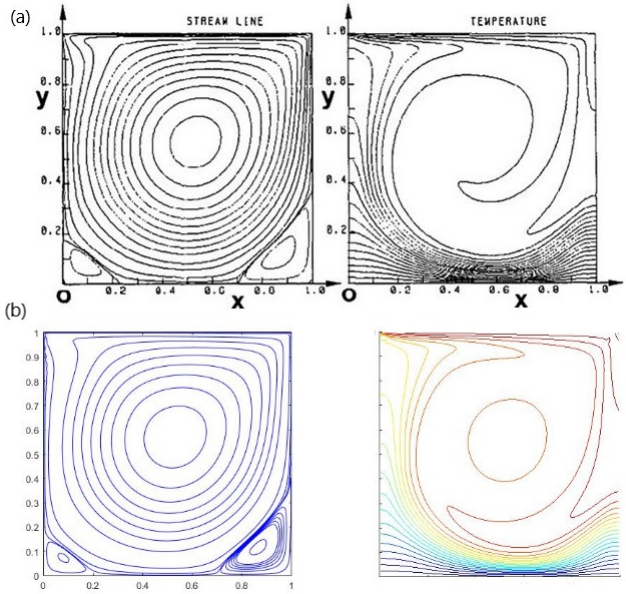

Figure 4: *Comparison of the Driven-cavity stream function between Iwatsu et al (a) and the present work (b) for $Re = 10^3$, $Gr = 10^2$*

$Re = 10^2$, and 10^3 at $Gr = 10^2$ when there is a lid driven cavity flow. The results closely agree with the Navier-Stokes results of Iwatsu et al [1].

The verification of the current algorithm is carried out in two folds. First, the present numerical solution is verified against two documented numerical studies. Namely, the numerical solutions reported by Iwatsu et al. [1] and Khanafer et al.[3], which is based on a finite volume scheme. The findings of the comparisons are documented in Tables (2) and (3) for the bounds on the magnitudes of the velocity components and the average Nusselt number predictions, respectively. Both comparisons illustrate close proximity in the predictions made between the various solutions. The second fold is a comparison between the predicted stream function contours under steady state condition of the present work to that of Khanafer et al. [3]. As displayed in figure (4), the comparison strikes an excellent agreement between both studies. Further validation case studies are documented in [1] and [3]. These validation cases boost the confidence in the numerical outcome of the present work.

III. Results and discussion

As stated earlier, the overall objective of the current investigation is to explore time dependent laminar mixed convection heat transfer in a lid-driven cavity. The implications of varying the Reynolds number, Grashof number and the lid oscillation frequency will be emphasized. The results are presented in terms of the temporal variation of the velocity and temperature profiles, streamline and isotherm patterns. The Reynolds number was varied between 10^2 and 10^3. In addition, the domain of Grashof number and dimensionless lid oscillation frequency were varied in the range of $10^2 \leq Gr \leq 10^6$, $0.1 \leq \omega \leq 5$ according to Khanafer et al [3], respectively. The study of the effect of the Reynolds number performed for values of $Gr = 100$ and $\omega = 0.5$. The usual dimensional speed components (v_x, v_y) and temperature T are plotted in the respective median sections of the cavity. The temporal variation of velocity and temperature profiles is presented for $Re = 10^2$ as shown in Figure (5). For positive lid velocity values $0 \leq t \leq \pi$,

	$Re = 10^2$			$Re = 10^3$		
	$(v_x/U_m)_{min}$	$(v_y/U_m)_{min}$	$(v_y/U_m)_{max}$	$(v_x/U_m)_{min}$	$(v_y/U_m)_{min}$	$(v_y/U_m)_{max}$
Iwatsu et al.	-0.2037	-0.2448	0.1699	-0.3781	-0.5178	0.4159
Khanafer et al.	-0.2093	-0.2482	0.1720	-0.3718	-0.5038	0.3588
present results	-0.2005	-0.2437	0.1637	-0.3598	-0.4810	0.3498

Table 2: *Comparison of the limits of velocity components between the present solution and other solutions at* $Gr = 10^2$

	$Gr = 10^2$		$Gr = 10^4$		$Gr = 10^6$	
	Iwatsu	*results*	*Iwatsu*	*Results*	*Iwatsu*	*Results*
$Re = 10^2$	1.94	1.97	1.34	1.61	1.02	1.02
$Re = 4.10^2$	3.84	3.84	3.62	3.60	1.22	1.21
$Re = 10^3$	6.33	6.30	6.29	6.30	1.77	1.80

Table 3: *Comparison of the average Nusselt number at the top wall between the present and Iwatsu solutions*

the mechanically induced shear force increases the force of the horizontal velocity. On the other hand, the speed of the cover modifies its sign once it enters the second half of the cycle $\pi \leq t \leq 2\pi$. As a result, the horizontal velocity component reverses the direction, therefore, loses much of its intensity in the vicinity of the lid region when confronted with the force-supported feedback action (buoyancy). The profile of the vertical speed component indicates a preferred increase in the first half of the speed cycle. The increase of Reynolds number to 1000, as shown in figure (6), brings about appreciated increase in the offered shear force and, subsequently, higher flow activities. Consequently, both velocity components register larger magnitudes in the bulk of the cavity. As a result, a greater flow penetration depth is achieved and the temperature profile is shown to depict significant convection heat transfer contribution to the overall energy transport process while conduction heat. the streamline and isotherm patterns due to the variation in Grashof number is presented for $Re = 10^2$ and $\omega = 1$. Figure (7) shows a primary vortex occupying a large part of the cavity for all the periods considered. This implies that the fluid is well mixed. We also note that the negative values of the cover speed cause the center of the vortex to move from right to left when the sliding cover changes direction. Furthermore, the intensity level of the line is weakened at this stage due to the apparent opposing forces of shear and buoyancy that hinder the penetration of the downward current. As a result, the isothermal patterns become laminated except in the vicinity of the sliding cover when $Re = 1000$ as shown in Figure (8), the flow is enhanced which facilitates the increase of the heat transfer process. This manifests that convective heat transfer has become the main energy vector in this case. In addition, the shear force provides a counter-reaction to the sustained buoyancy effect for the negative velocity of the lid, as previously indicated. Due to the overwhelming effect of the existing shearing force, the two secondary vortices's are observed to be displayed on the upper sides of the cavity. The isotherms are therefore grouped near the bottom wall, indicating the existence of high temperature gradients in the vertical direction.

The streamline and isothermal profiles due to the variation of the Grashof number are shown in figures (9) and (10) for $Re = 10^2$, $\omega = 1$ and $0 \leq t \leq 2\pi$. As the number of Grashof increases, the intensity of convection intensifies in the cavity due to the increase in buoyancy effect. This is evident from the substantial flow increase in the cavity at different times. The buoyancy effect facilitates flow in the positive velocity cycle while counteracting

the shear effect in the negative velocity cycle. This is demonstrated by figure (9) from the existence of a secondary vortex near the top wall for the negative oscillation conditions of the lid. The secondary vortex is clearly visible at the negative oscillation rate for a relatively small Reynolds number value. In addition, the calculated isotherms are qualitatively similar to the steady state solution of mixed convection induced cavity flows under positive oscillation velocity conditions.The swing lid counteracts the effect of natural convection, which hinders heat transfer activities and primarily forces to conduction. As the Grashof number increases to 10^6, the primary swirl cell splits into smaller swirls due to a high buoyancy effect that exceeds the effect of oscillation velocity, as shown in figure (10). In addition, the isothermal plotted for the oscillation rates indicate a significant decrease in the contribution of convective heat transfer to the overall rate of heat transfer over $Gr = 10^2$. Figure (11) shows that for small values of Grashof number $Gr = 10^2$ the main vortex moves towards the cavity center when the Reynolds number increases, because the effect of forced convection is dominant. However,when the Grashof number becomes more important, the vortex that appears does not penetrate into the cavity. It remains near the upper wall, because of the buoyancy effect becomes stronger. Heat transfer as shown in figure (12) is important for low Grashof number values and high Reynolds number values, on the contrary when the Grashof number increases the rate of heat transfer decreases.

Figure (13) shows the variation of the oscillation frequency for $Re = 10^2$, 10^3 at $Gr = 10^2$. This presents the streamlines for ω, and implies that the incorporation of a relatively low value ω ($\omega = 0.1$) facilitates the predominance of shear on the effect of buoyancy. This will therefore allow additional penetration of the flow associated with the cover down into the cavity at the expense of the movement generated by the buoyancy. Such a scenario is reversed when larger ($\omega = 5$). The buoyancy effect becomes more pronounced (the appearance of secondary vortices's) because it seems to limit the effectiveness of the shear force at a close distance from the sliding cover. Apparently, increasing ω reduces the downward effect of lid movement on the fluid. It is interesting to note that when the normalized frequency is relatively small, the increase in convective heat transfer is apparent under this condition shown in figure (14) . As the frequency value increases, the excitation of fluid movement provided by the sliding cover is limited to a low fluid depth. This causes the fluid to become substantially immobile in most of the inner region. As a result, the heat transfer process decreases in this situation. The results for the variation of oscillation frequency for $Gr = 10^2$ and 10^6 at $Re = 10^2$ is shown in Figures (15).

This implies that the incorporation of a value ω ($\omega = 0.1$) relatively weak facilitates the predominance of shear on the effect of buoyancy. As ω and Gr become larger, the buoyancy effect becomes larger. Increasing ω and Gr clearly reduces the downward effect of lid movement on the fluid. Figure (16) shows that when the frequency value and Gr increase, we do observe the same phenomenon as in $Fig.(14)$. The number of local Nusselt with the hot upper wall decreases as a function of time, unlike the cold bottom wall it increases slightly until it reaches a fixed value (stability) for different values of Re as it is shown on figures (17).

The Reynolds number effect on the Nusselt number is shown in the figure (18), the results showing that when the increase in Re the Nu increases also for the upper and lower walls, this is due to the high effect of the shear force, we also see that the Nu along the upper wall decreases as a function of time. It is the opposite for the lower wall the increased Nu, these results can be explained by the fluid mixture, which results in the convective heat transfer between the two walls. As shown in Figure (18), the Nusselt number of upper wall increases as a function of Reynolds number, which indicates increased heat transfer with Reynolds number. Flow through a moving wall is assumed to be compared to laminar flow on a flat plate. The Blasius equation giving the orders of magnitude of the dimensional thermal

boundary layer (δ) at a distance y is given by:

$$\delta = Re^{-1/2}.y \tag{20}$$

Where (δ) is the displacement thickness. The curve seems to be a linear curve for Reynolds values $(Re \geq 500)$, the variation of the heat transfers represented by the Nusselt number $(Nu \approx 1/\delta)$:

$$Nu \approx Re^{1/2} \tag{21}$$

The adjusted Nusselt number is given by:

$$Nu = 0.25 \times Re^{0.462} \tag{22}$$

Figure (19) shows the mean number of Nu Nusselt as a function of the buoyancy forces (Gr) and the movement driven by the cover (Re).The curve clearly indicates that heat transfers decrease significantly with forced convection when $Gr^2 < Re$. After that there is a small increase in transfer rate with natural convection when $Gr^2 > Re$. The effect of frequency variation on the Nusselt number is shown in Figure (20). There is a decrease in Nusselt number depending on the frequency. The adjusted Nusselt number is given by:

$$Nu = 1.8 \times \omega^{-0.2} \tag{23}$$

Evolution The number of Nusselt is given as:

$$Nu \approx \omega^{-1/5} \tag{24}$$

It is noted that the decrease of Nu is very strong for small values of the frequency, but for values of greater frequency the number of Nusselt varies slightly, due to the increase of the effect of the buoyancy force, so the fluid is well mixed.

IV. Conclusion

The LBM moment model was applied to simulate mixed flow in a square cavity. External excitation was imposed on the movement of the lid. The study was conducted for a number of relevant dimensionless groups, namely the Reynolds number (Re = 100, 400 and 1000), the Grashof number ($Gr = 10^2$, 10^4 and 10^6) and the dimensionless oscillation frequency of the sliding cover (ω = 0.1, 1 and 5). The obtained results present stable periodic solutions. Such results show that the Reynolds number and the Grashof number have a profound effect on the structure of the fluid flow and the heat transfer of the fields. In fact, their effects are associated with the direction of the sliding lid. In addition, the results indicate that the shear force imposed on the sliding cover increases with increasing Reynolds number and lid frequency and it decreases as the Grashof number increases. The number of local Nusselt at the top wall heats starts with a high value especially for high values of Reynolds number and then decreases rapidly. thus for cold bottom wall The number of Nusselt shows an increase. When the Grashof number is large relative to a constant Reynolds number, the flow rate changes from forced convection to natural convection. However, the number of Nusselt decreases according to Grashof number. On the contrary, when the Grashof number is constant, the Reynolds number has a large effect on the Nusselt number. So, the forced convection dominates the flow. In the context of the Reynolds, Grashof numbers and frequencies studied in this article, two trends are obtained to evaluate the evolution of Nusselt numbers. Induced heat transfer depends on $Gr^{-1/12}$, $Re^{1/2}$ or $\omega^{-1/5}$, respectively dominating natural convection and forced convection.

References

[1] Reima Iwatsu, Jae Min Hyun, and Kunio Kuwahara. Mixed convection in a driven cavity with a stable vertical temperature gradient. *International Journal of Heat and Mass Transfer*, 36(6):1601 – 1608, 1993.

[2] A. K. Prasad and J. R. Koseff. Reynolds number and end-wall effects on a lid-driven cavity flow. *Physics of Fluids*, 1:208–218, February 1989.

[3] Khalil M. Khanafer, Abdalla M. Al-Amiri, and Ioan Pop. Numerical simulation of unsteady mixed convection in a driven

cavity using an externally excited sliding lid. 26(5):669 – 687.

[4] DE Ameziani, Y Guo, R Bennacer, Mohammed El Ganaoui, and M Bouzidi. Competition between lid driven and natural convection in square cavity: lattice boltzmann method. In *International Symposium in Computational Heat Transfer (CHT'08)*, pages 20–pages. Begell House.

[5] Samir Houat and Zine Elabidine Bouayed. The lattice boltzmann method for mixed convection in a cavity. 139:186 – 191.

[6] Eduardo Ramos, Brian D. Storey, Fernando Sierra, RaÃžl A. ZÃžÃśiga, and Andriy Avramenko. Temperature distribution in an oscillatory flow with a sinusoidal wall temperature. *International Journal of Heat and Mass Transfer*, 47(22):4929 – 4938, 2004.

[7] Siva Subrahmanyam Mendu and P. K. Das. Fluid flow in a cavity driven by an oscillating lid a simulation by lattice boltzmann method. 39:59 – 70.

[8] Natalia Vladimirova, Andrea Malagoli, and Roberto Mauri. Two-dimensional model of phase segregation in liquid binary mixtures. *Physical Review E*, 60(6):6968, 1999.

[9] Domenico Suppa, Olga Kuksenok, Anna C Balazs, and JM Yeomans. Phase separation of a binary fluid in the presence of immobile particles: A lattice boltzmann approach. *The Journal of chemical physics*, 116(14):6305–6310, 2002.

[10] Aiguo Xu, G Gonnella, and A Lamura. Phase-separating binary fluids under oscillatory shear. *Physical Review E*, 67(5):056105, 2003.

[11] Xiaowen Shan and Gary Doolen. Multicomponent lattice-boltzmann model with interparticle interaction. *Journal of Statistical Physics*, 81(1-2):379–393, 1995.

[12] P Raiskinmäki, A Koponen, J Merikoski, and J Timonen. Spreading dynamics of three-dimensional droplets by the lattice-boltzmann method. *Computational Materials Science*, 18(1):7–12, 2000.

[13] Dai Iwahara, Hiroyuki Shinto, Minoru Miyahara, and Ko Higashitani. Liquid drops on homogeneous and chemically heterogeneous surfaces: A two-dimensional lattice boltzmann study. *Langmuir*, 19(21):9086–9093, 2003.

[14] Bruce J Palmer and David R Rector. Lattice-boltzmann algorithm for simulating thermal two-phase flow. *Physical Review E*, 61(5):5295, 2000.

[15] Anthony JC Ladd. Numerical simulations of particulate suspensions via a discretized boltzmann equation. part 1. theoretical foundation. *Journal of fluid mechanics*, 271:285–309, 1994.

[16] Anthony JC Ladd. Numerical simulations of particulate suspensions via a discretized boltzmann equation. part 2. numerical results. *Journal of fluid mechanics*, 271:311–339, 1994.

[17] S Succi, E Foti, and F Higuera. Three-dimensional flows in complex geometries with the lattice boltzmann method. *EPL (Europhysics Letters)*, 10(5):433, 1989.

[18] Anton WJ Heijs and Christopher P Lowe. Numerical evaluation of the permeability and the kozeny constant for two types of porous media. *Physical Review E*, 51(5):4346, 1995.

[19] Frank J Alexander, Shiyi Chen, and JD Sterling. Lattice boltzmann thermohydrodynamics. *Physical Review E*, 47(4):R2249, 1993.

[20] Xiaoyi He, Shiyi Chen, and Gary D Doolen. A novel thermal model for the lattice boltzmann method in incompressible limit. *Journal of Computational Physics*, 146(1):282–300, 1998.

[21] GH Tang, WQ Tao, and YL He. Simulation of fluid flow and heat transfer in a plane channel using the lattice boltzmann method. *International Journal of Modern Physics B*, 17(01n02):183–187, 2003.

[22] Elalami Semma, Mohammed El Ganaoui, R Bennacer, and AA Mohamad. Investigation of flows in solidification by using the lattice boltzmann method. *International Journal of Thermal Sciences*, 47(3):201–208, 2008.

[23] Guy McNamara and Berni Alder. Analysis of the lattice boltzmann treatment of hydrodynamics. *Physica A: Statistical Mechanics and its Applications*, 194(1-4):218–228, 1993.

[24] Y Chen, H Ohashi, and M Akiyama. Thermal lattice bhatnagar-gross-krook model without nonlinear deviations in macrodynamic equations. *Physical Review E*, 50(4):2776, 1994.

[25] Raoyang Zhang and Hudong Chen. Lattice boltzmann method for simulations of liquid-vapor thermal flows. *Physical Review E*, 67(6):066711, 2003.

[26] Ahmed Mezrhab, Mohammed Jami, M'hamed Bouzidi, and Pierre Lallemand. Analysis of radiation–natural convection in a divided enclosure using the lattice boltzmann method. *Computers & Fluids*, 36(2):423–434, 2007.

[27] Dominique d'Humieres. Generalized lattice-boltzmann equations. *Rarefied gas dynamics*, 1992.

[28] Ahmed Mezrhab, M'hamed Bouzidi, and Pierre Lallemand. Hybrid lattice-boltzmann finite-difference simulation of convective flows. *Computers & Fluids*, 33(4):623–641, 2004.

[29] Mohamed Mahdi Tekitek, M Bouzidi, François Dubois, and Pierre Lallemand. Adjoint lattice boltzmann equation for parameter identification. *Computers & fluids*, 35(8-9):805–813, 2006.

[30] PN Shankar and MD Deshpande. Fluid mechanics in the driven cavity. *Annual review of fluid mechanics*, 32(1):93–136, 2000.

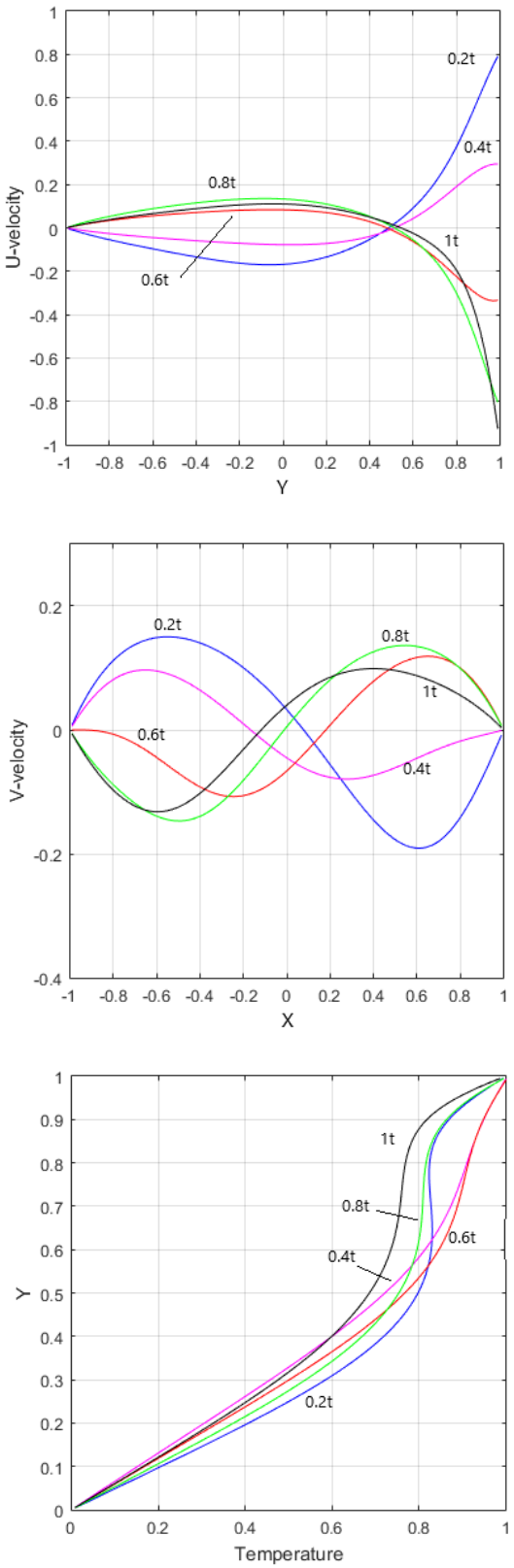

Figure 5: *Variation of the velocity and vertical temperature profiles at the respective mid sections for* $Re = 10^2$, $Gr = 10^2$ *and* $\omega = 1$

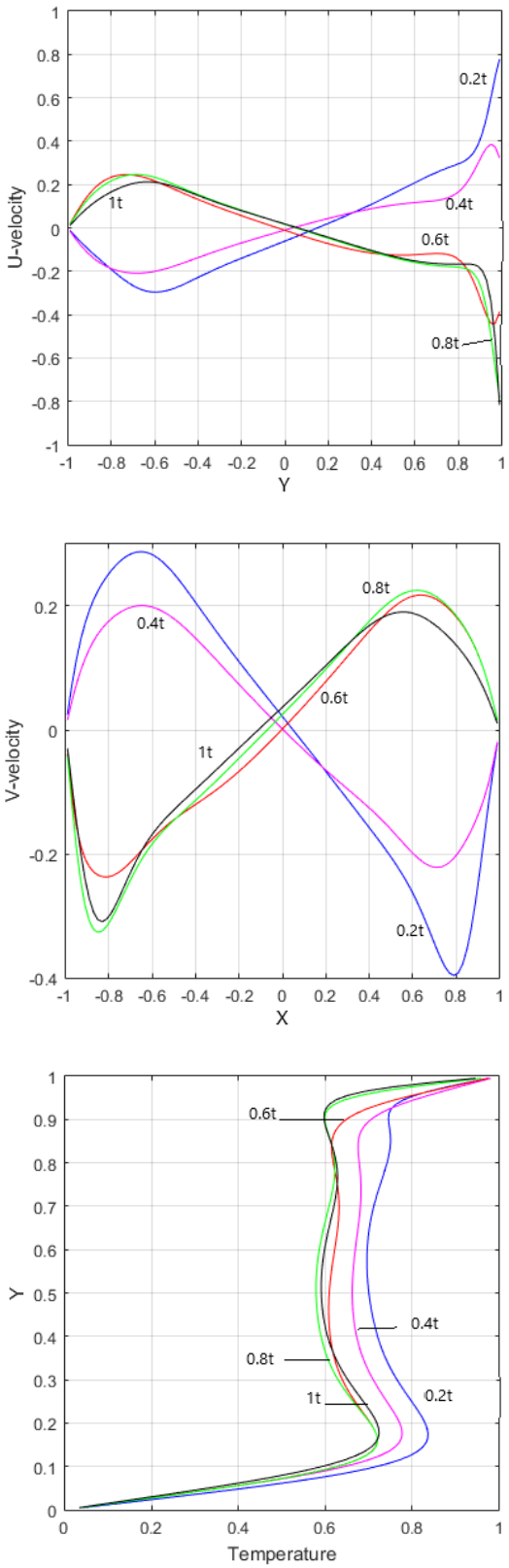

Figure 6: *Variation of the velocity and vertical temperature profiles at the respective mid sections for* $Re = 1000$, $Gr = 10^2$ *and* $\omega = 1$

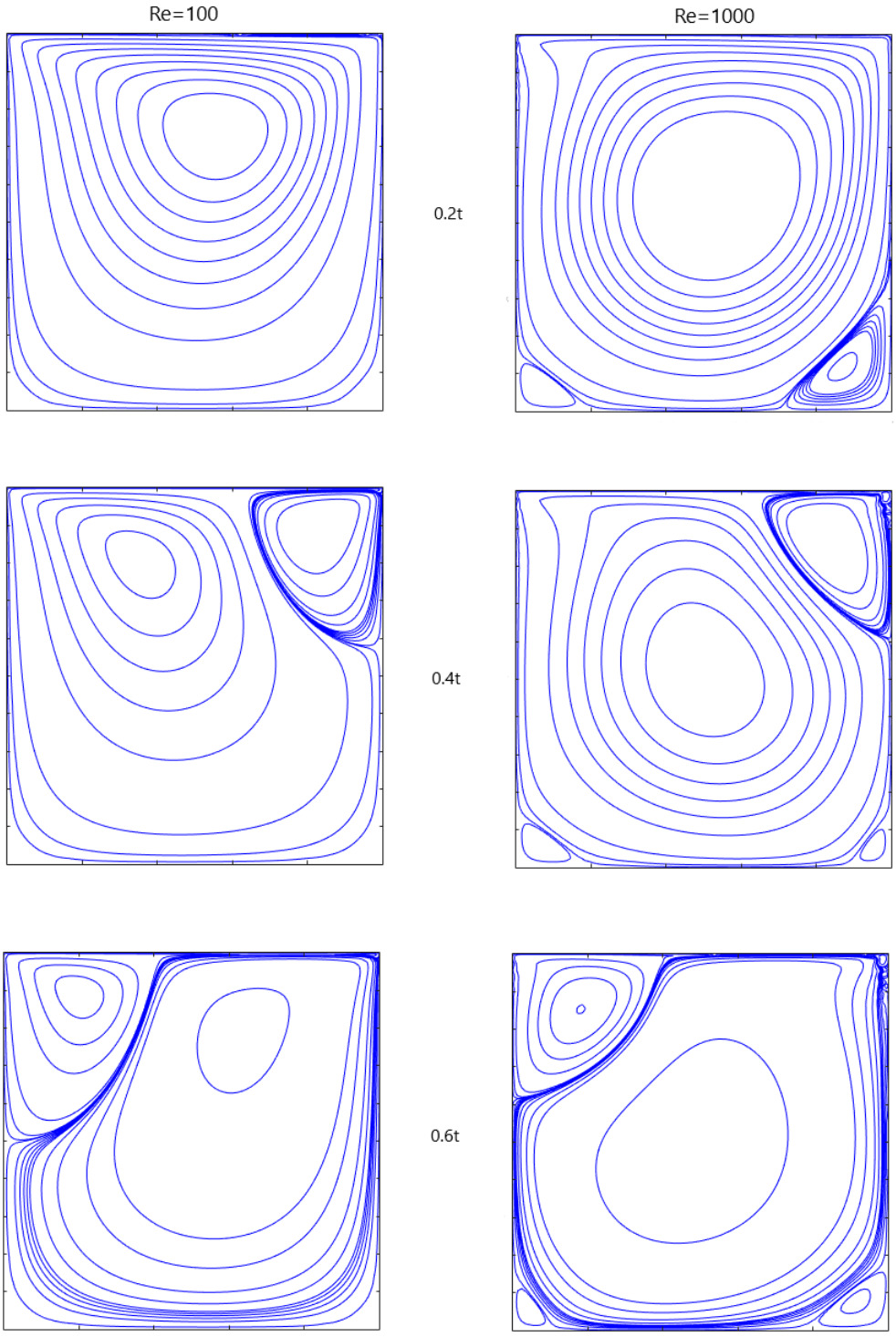
Re=100
Re=1000
0.2t
0.4t
0.6t

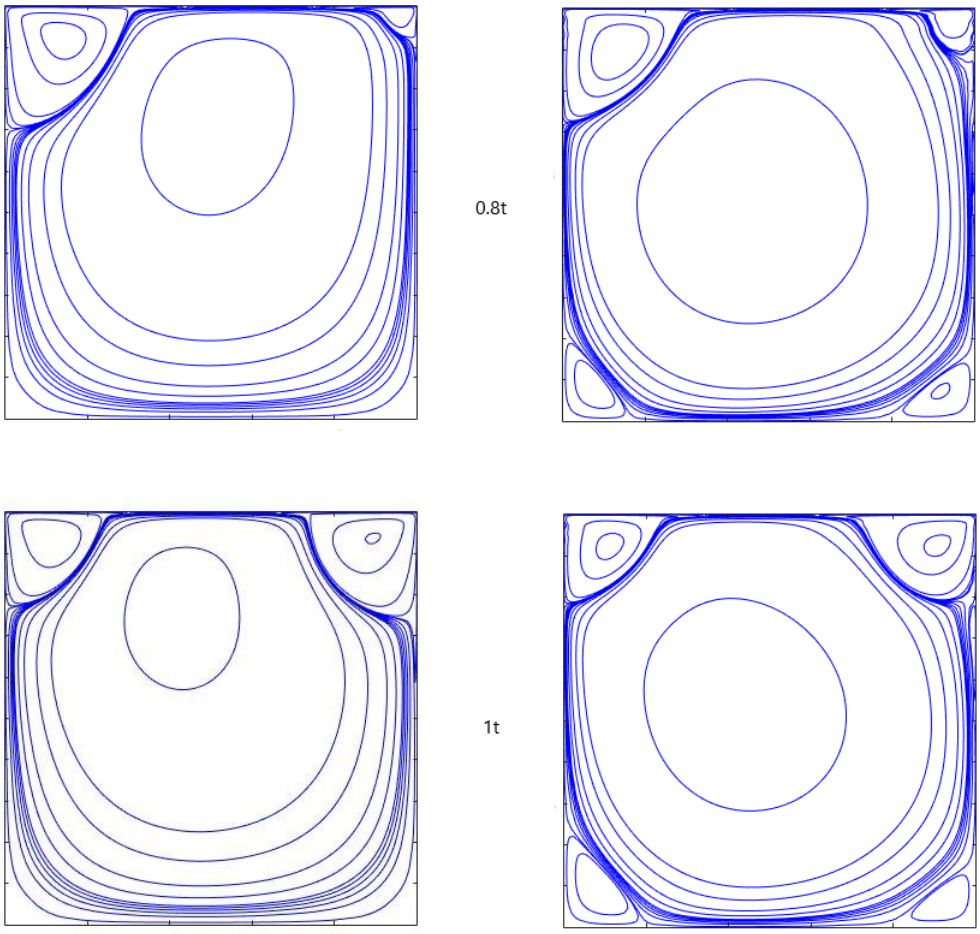

Figure 7: *Variation of the streamline contours for* $Re = 100$ *and* 1000 *at deferents periods*

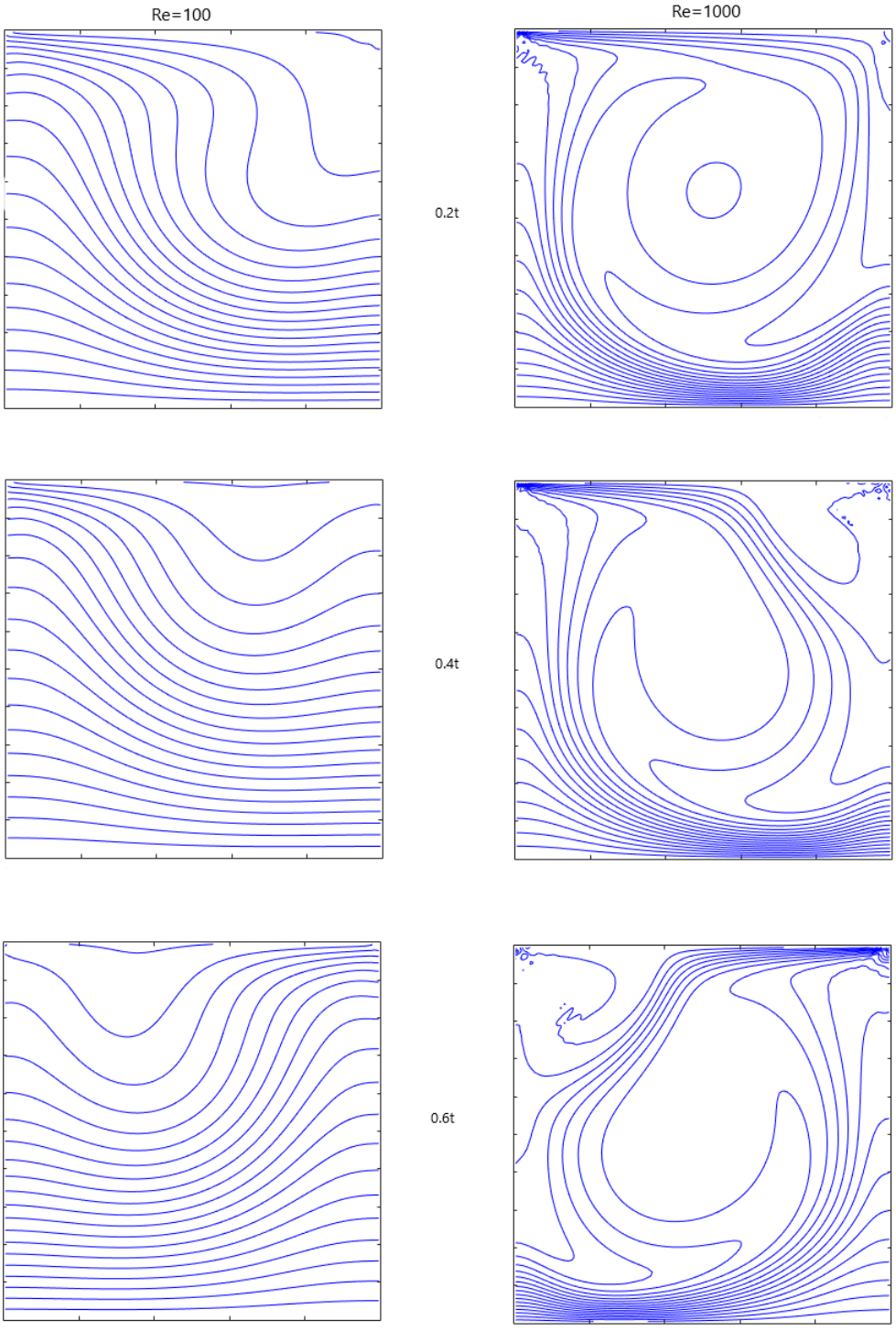
Re=100
Re=1000
0.2t
0.4t
0.6t

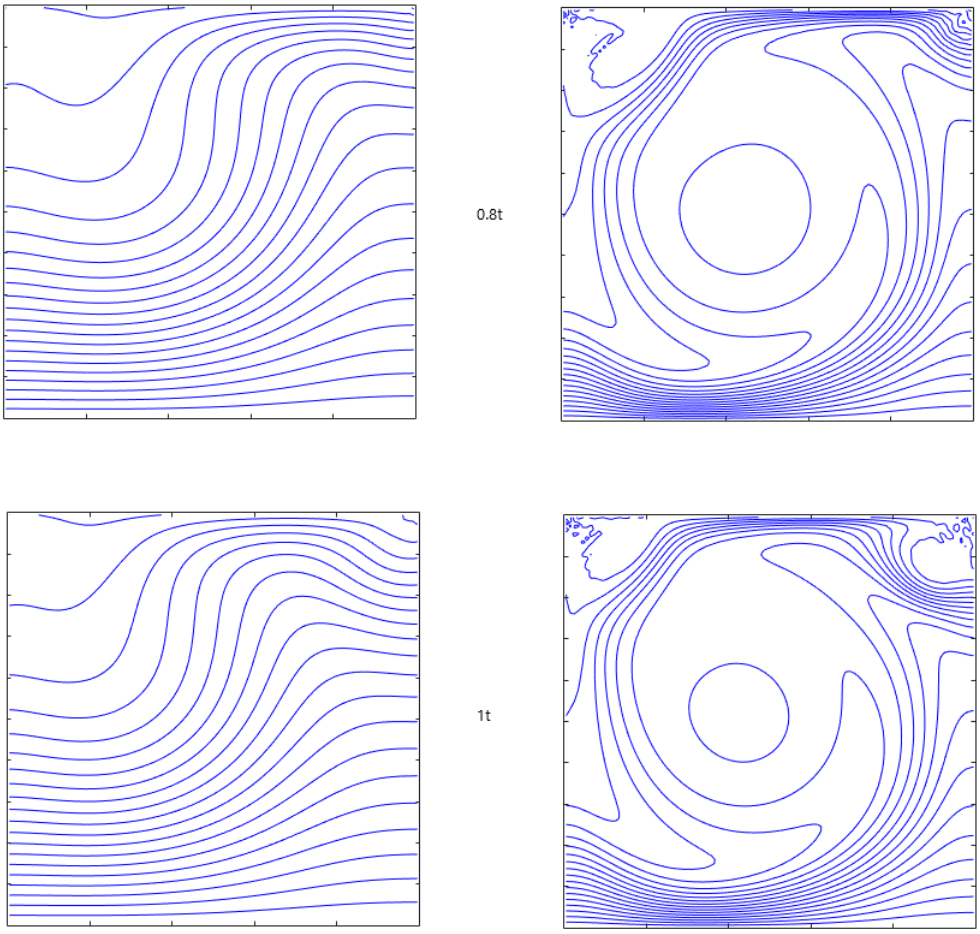

Figure 8: *Variation of the isotherm contours for* $Re = 100$ *and* 1000 *at deferents periods*

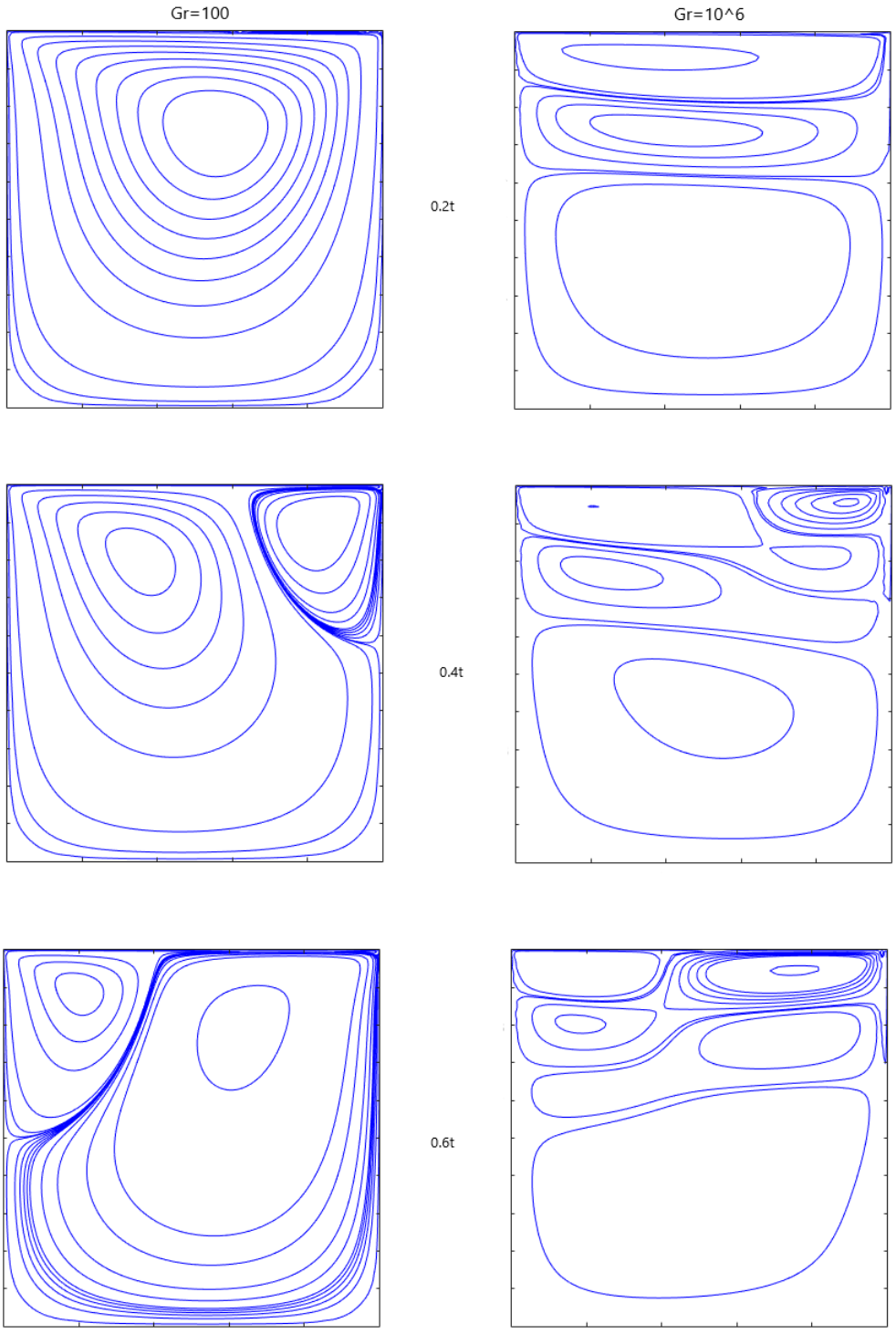
Gr=100
Gr=10^6
0.2t
0.4t
0.6t

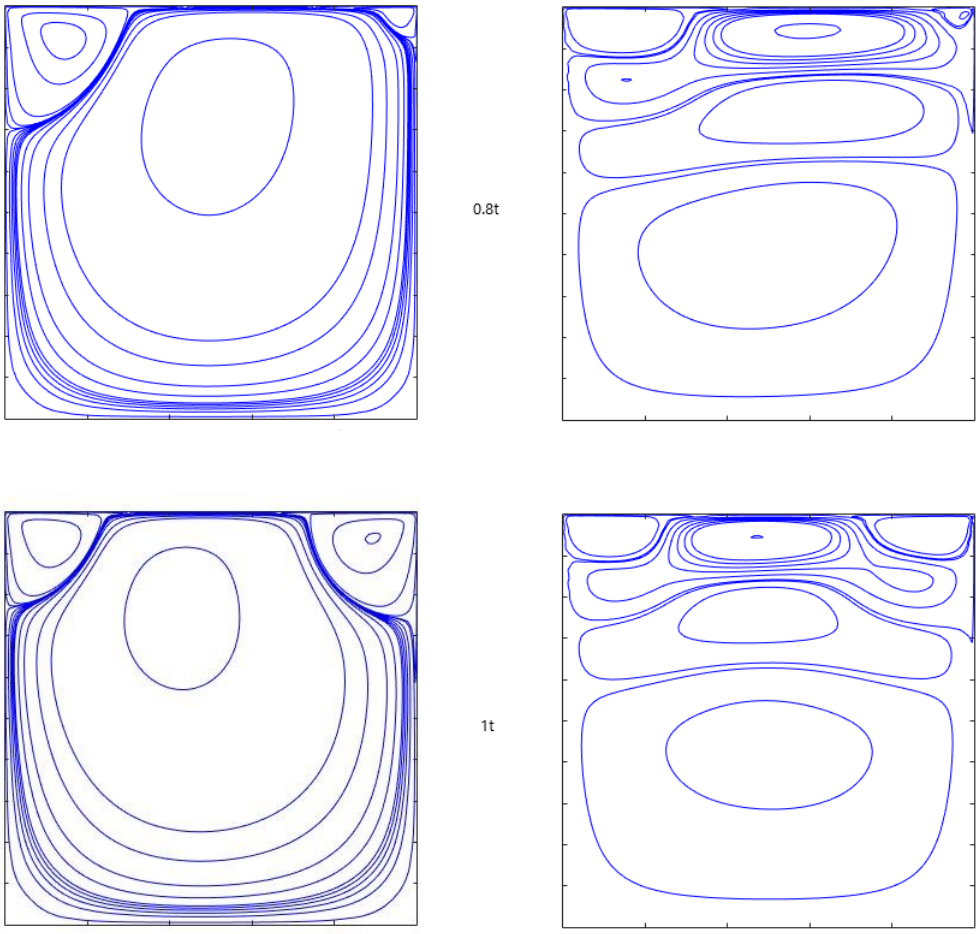

Figure 9: *Variation of the streamline contours for* $Gr = 10^2$ *and* 10^6 *at deferents periods*

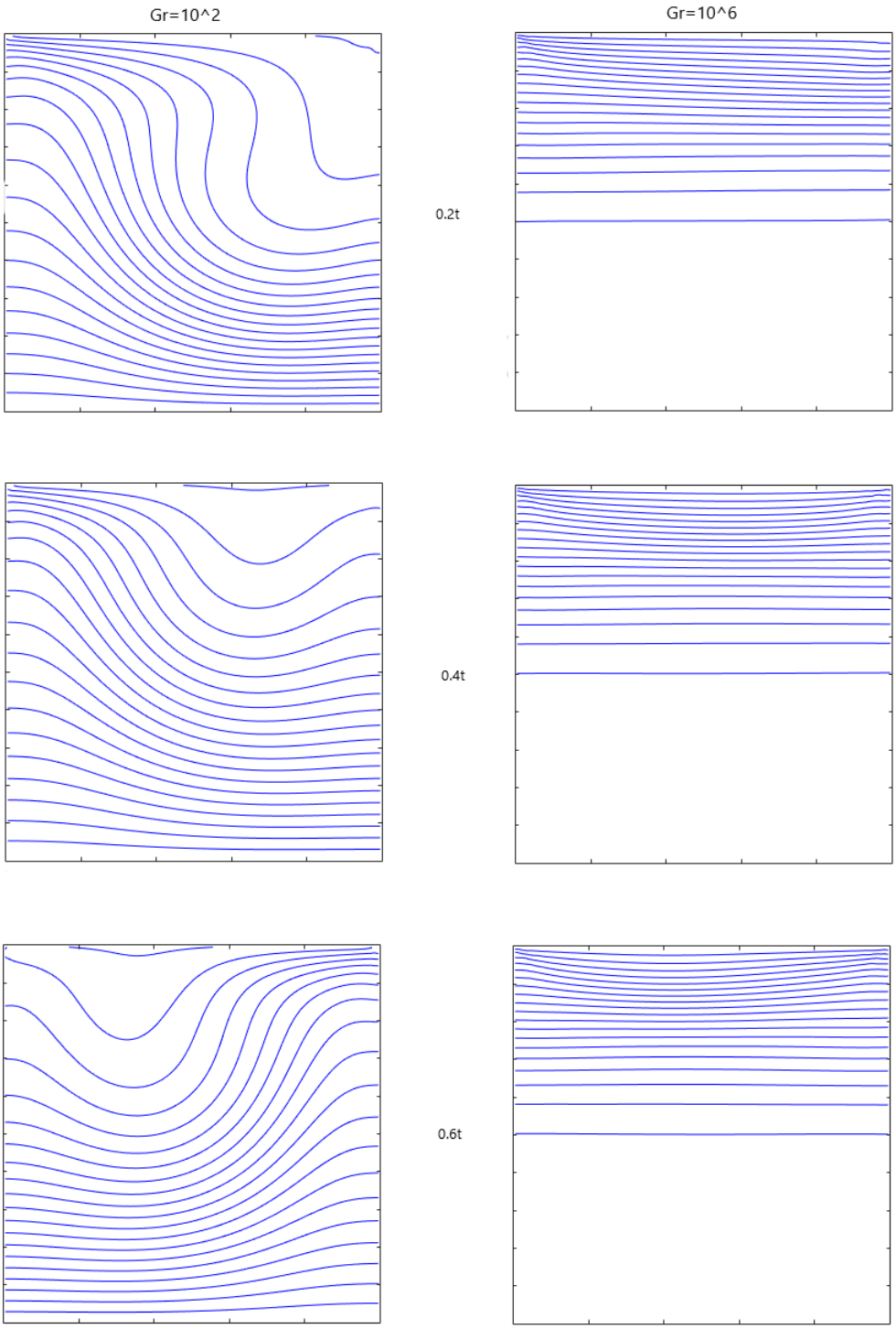
Gr=10^2
Gr=10^6
0.2t
0.4t
0.6t

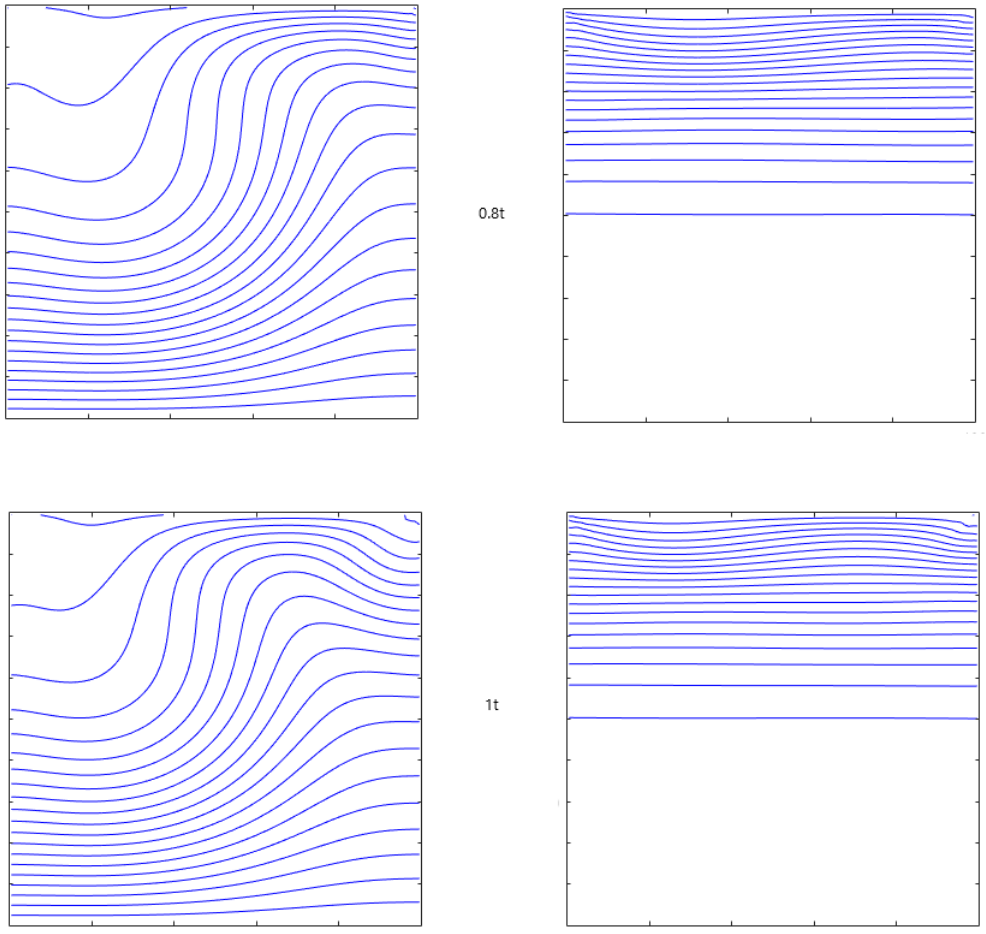

Figure 10: *Variation of the isotherm contours for* $Gr = 10^2$ *and* 10^6 *at deferents periods*

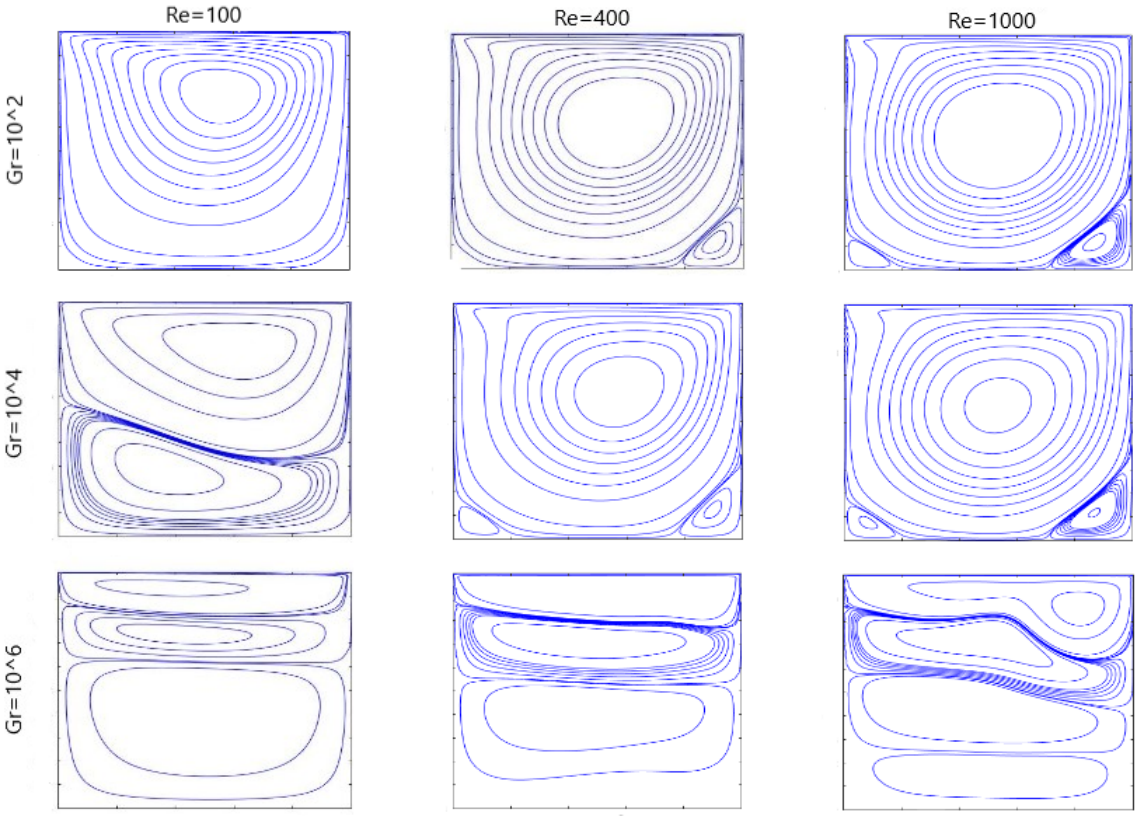

Figure 11: *Variation of the streamlines for different values Re and Gr at* $\omega = 1$

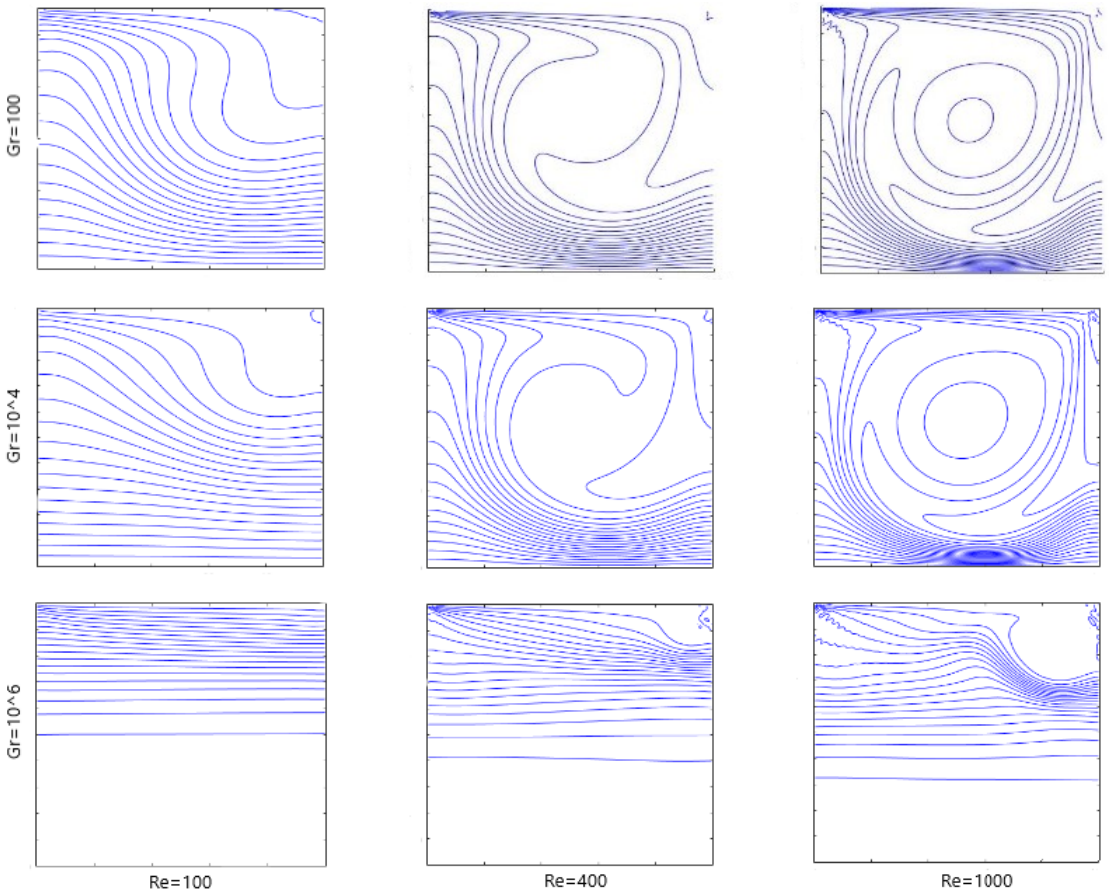

Figure 12: *variation of the isotherms contours for different values Re and Gr at* $\omega = 1$

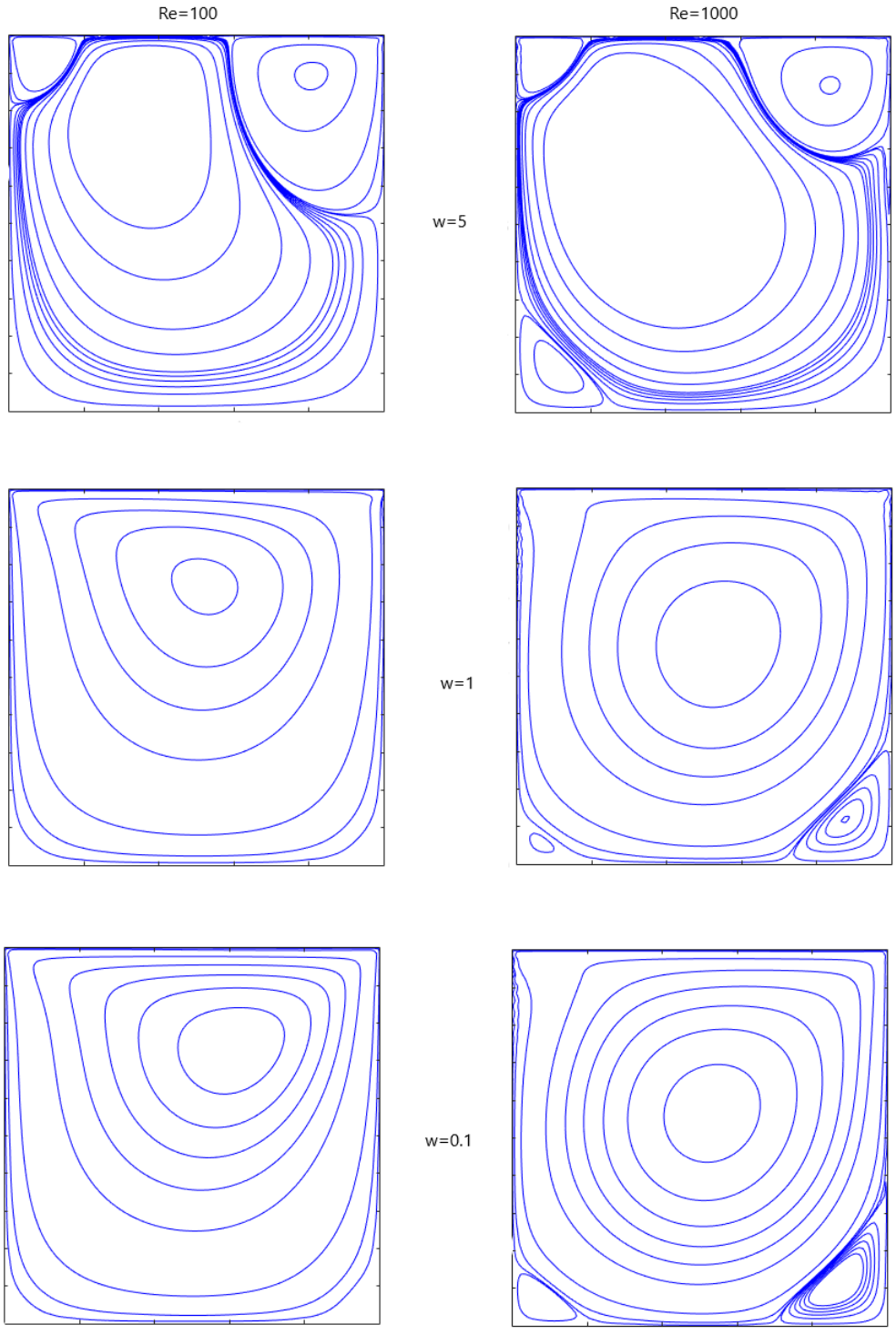

Figure 13: *Variation of the streamlines contours for different frequency and Reynolds number* $Re = 10^2$ *and* 10^3

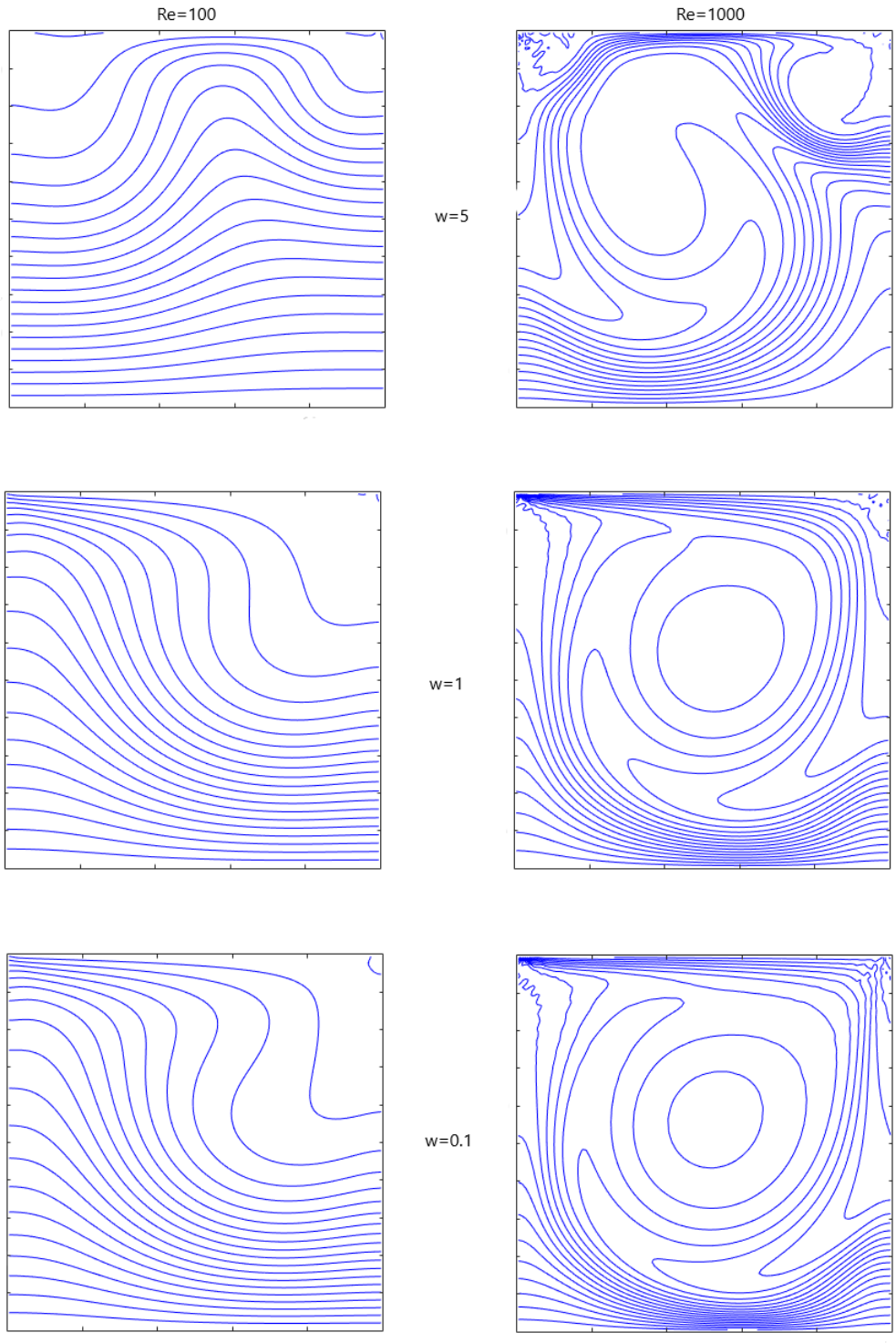

Figure 14: *Variation of the isotherms contours for different frequency and Reynolds number* $Re = 10^2$ *and* 10^3

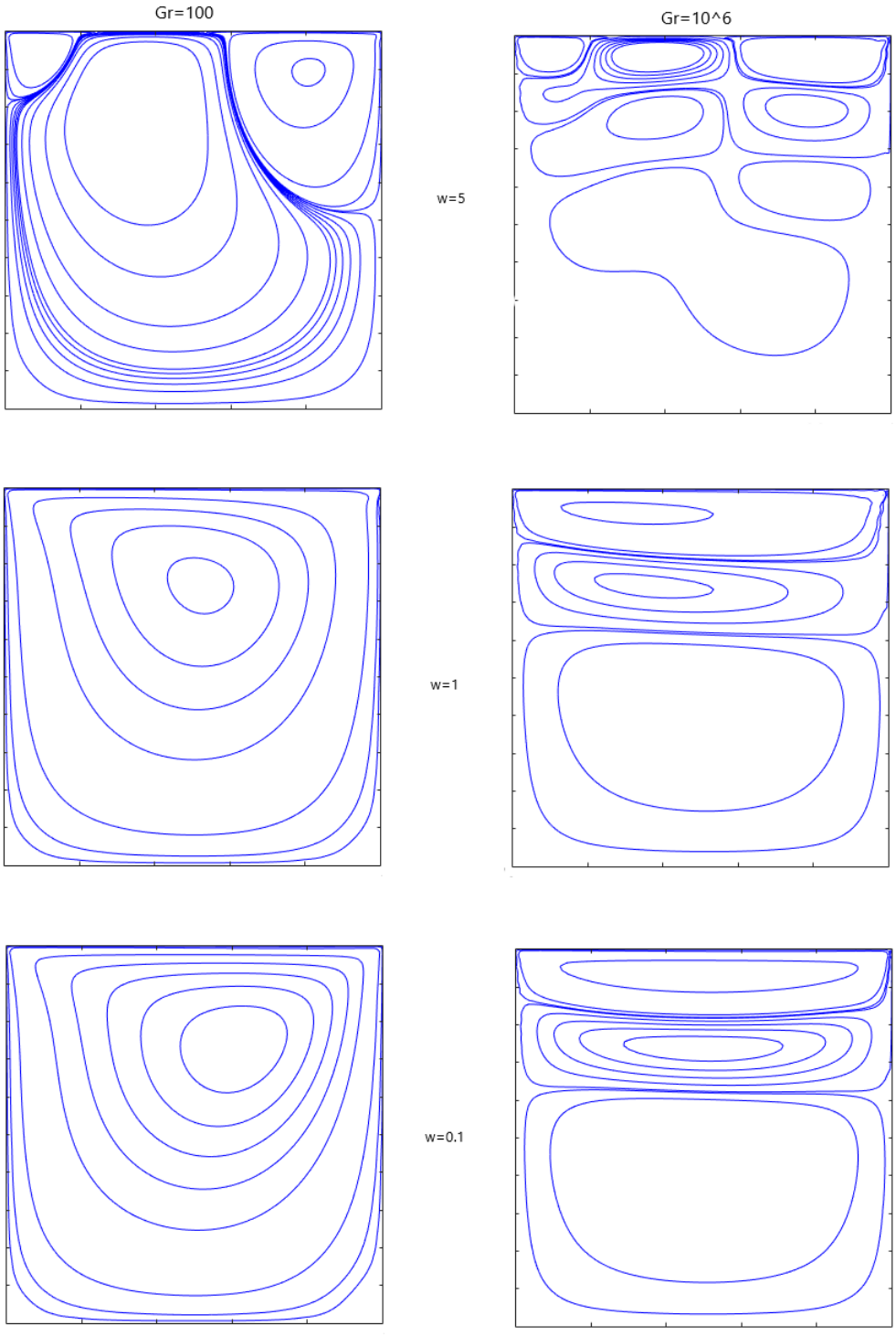

Figure 15: *Variation of the streamlines contours for different frequency and Grashof number* $Gr = 10^2$ *and* $Gr = 10^6$

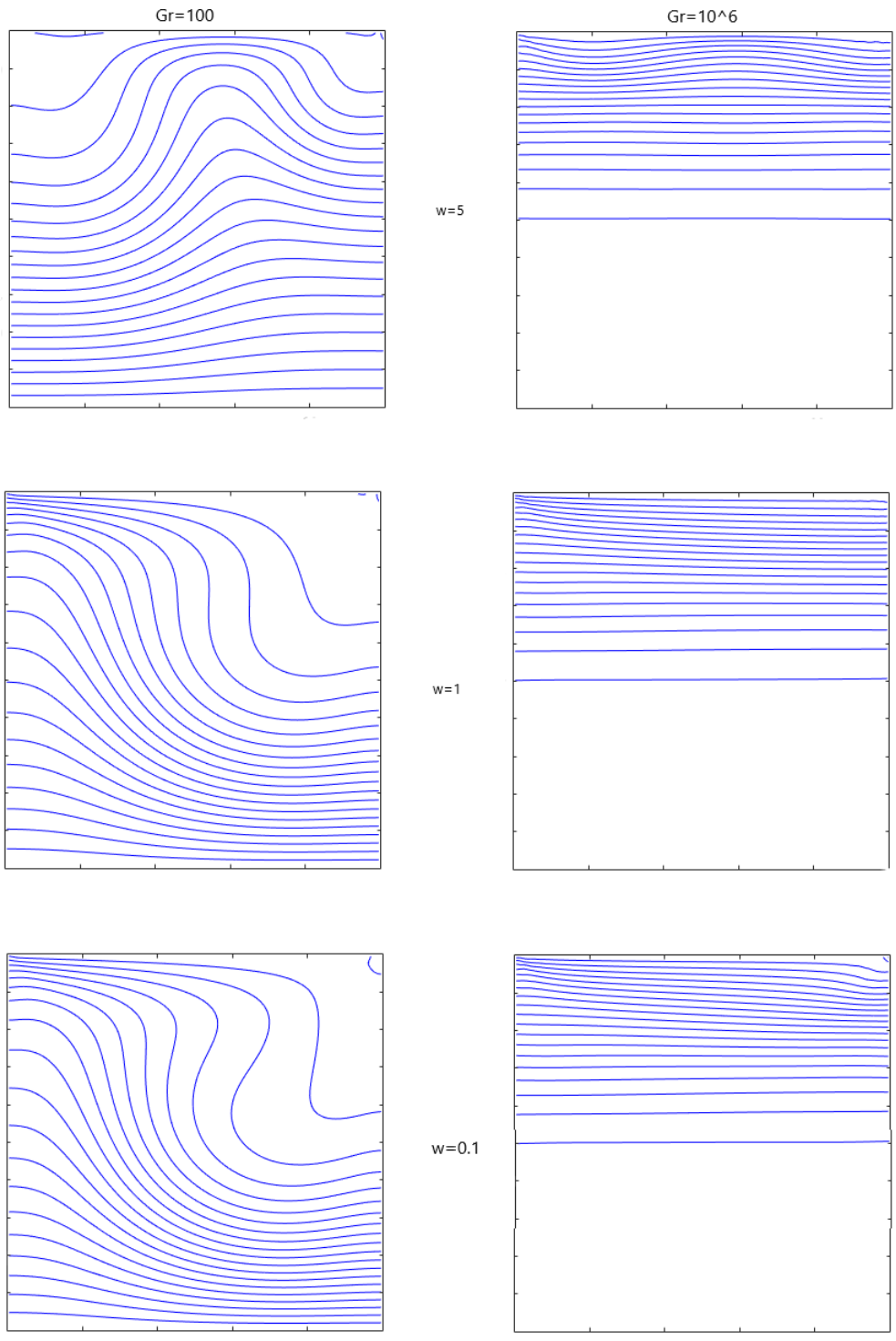

Figure 16: *Variation of the isotherms contours for different frequency and Grashof number* $Gr = 10^2$ *and* 10^6

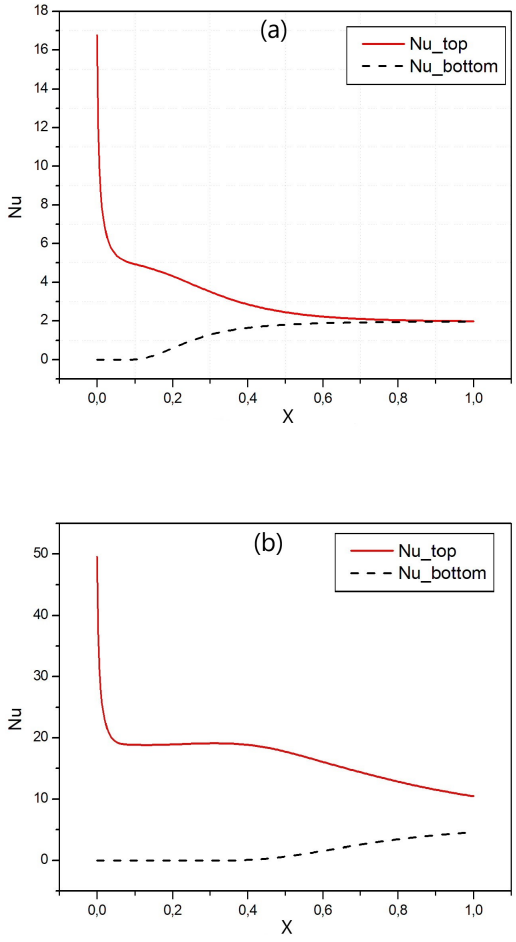

Figure 17: *Nusselt number at upper and bottom wall for* $Re = 100$ (a) *and* $Re = 1000$ (b)

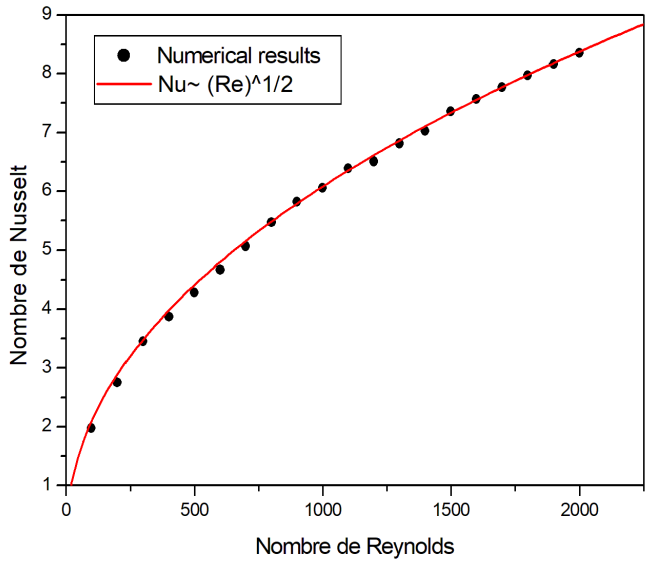

Figure 18: *Nusselt number at different Reynolds numbers at* $Gr = 100$ *and* $\omega = 0.5$

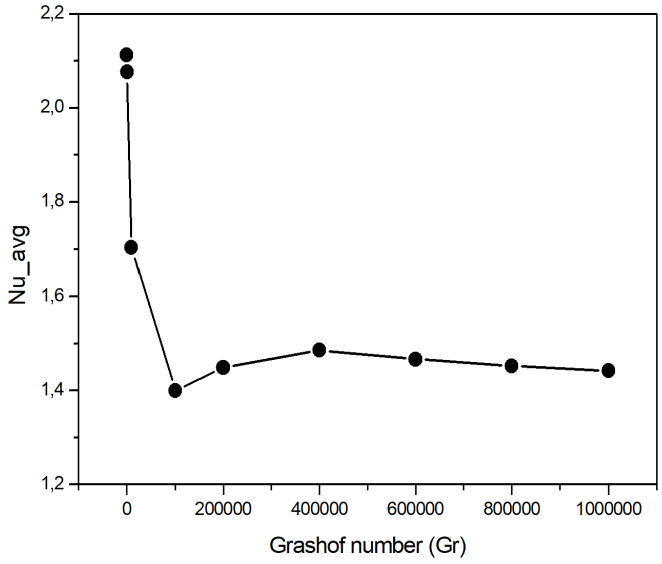

Figure 19: *Number of Nusselt at different Grashof number at* $Re = 100$ *and* $\omega = 0.5$

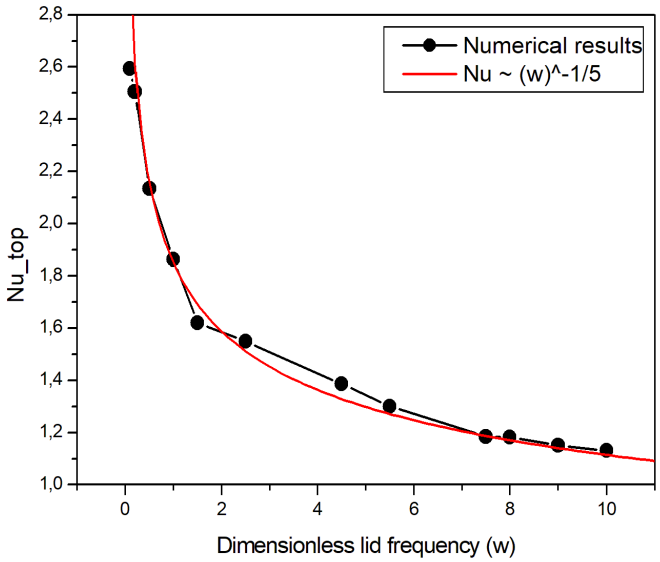

Figure 20: *Nusselt number at upper wall for different frequency at* $Re = 100$ *and* $Gr = 100$